

A Compact Substrate Integrated Waveguide Notched-Septum Polarizer for 5G Mobile Devices

Khaled Al-Amoodi, Rashid Mirzavand, Mohammad Mahdi Honari, Jordan Melzer, Duncan G. Elliott, Pedram Mousavi

K. Al-Amoodi, R. Mirzavand, M. M. Honari, J. Melzer, D. G. Elliott and P. Mousavi, "A Compact Substrate Integrated Waveguide Notched-Septum Polarizer for 5G Mobile Devices," in IEEE Antennas and Wireless Propagation Letters, vol. 19, no. 12, pp. 2517-2521, Dec. 2020, doi: 10.1109/LAWP.2020.3038404

IEEE Xplore, <https://ieeexplore.ieee.org/document/9261097>

Compact Substrate Integrated Waveguide Notched-Septum Polarizer for 5G Mobile Devices

Khaled Al-Amoodi, Rashid Mirzavand, Mohammad Mahdi Honari, Jordan Melzer, Duncan G. Elliott, and Pedram Mousavi

Abstract—In this letter, a compact substrate-integrated waveguide notched-septum polarizer is designed, manufactured and tested. Metalized slots are used instead of vias in proximity to the notches to improve polarization purity. An impedance matching bandwidth of 7.9% at 29 GHz and transmission coefficient of better than -1.6 dB are demonstrated. The axial ratio is less than 3 dB over a bandwidth of 4.5% at 29 GHz (sufficient for 5G). An implementation of the polarizer in an array antenna was measured to validate its reliability in antenna applications. Given its performance and small form-factor (length of $\lambda_o/7$ at 29 GHz), the proposed polarizer may be a good option for SIW circularly polarized endfire antennas in 5G mobile devices.

Index Terms—Compact, dual circular polarization (CP), millimeter-wave (mmWave), notched, septum polarizer, substrate integrated waveguide (SIW).

I. INTRODUCTION

THE capability to generate circular polarization (CP) introduces robustness to fading and misalignment in polarization which would otherwise reduce signal reception. This is especially important for 5G devices [1]. Furthermore, it must be done within the space constraint of mobile devices. While it may be exciting to design for large bandwidths of operation, it is unreasonable to design for performance beyond the intended use (such as the 3% band at 28 GHz for 5G), especially at the cost of size. Alternating horizontally- and vertically-polarized antennas (such as in [2], [3]) can provide dual linear polarization for polarization diversity, but requires twice as many elements. Waveguide polarizers using irises [4] show great CP performance, but are complex to manufacture in a PCB process. Septum-based polarizers are easy to design and are tolerant to manufacturing variations. Furthermore, they achieve wide axial ratio (AR) bandwidths; however, they also are quite large (with lengths of $1.7\lambda_o$ [5], $1.5\lambda_o$ [6], $0.7\lambda_o$ [7] and $1.2\lambda_o$ [8]). Designing in substrate integrated waveguides (SIWs) is beneficial due to their smaller size and ease of manufacture in standard PCB processes, which are two necessities for 5G applications [9], [10].

Manuscript received January 0, 0000; revised January 0, 0000; accepted January 0, 0000. Date of publication January 0, 0000; date of current version January 0, 0000. This work was supported by the Natural Sciences and Engineering Research Council (NSERC) and CMC Microsystems. (Corresponding author: Khaled Al-Amoodi.)

J. Melzer is with Telus Communications, Ottawa ON K1P 0A6, Canada (e-mail: jordan.melzer@telus.com).

K. Al-Amoodi, R. Mirzavand, M. M. Honari, D. G. Elliott, and P. Mousavi are with the Department of Electrical and Computer Engineering, University of Alberta, Edmonton AB T6G 1H9, Canada (e-mail: kalamood@ualberta.ca, mirzavan@ualberta.ca, honarika@ualberta.ca, Duncan.Elliott@ualberta.ca, pmousavi@ualberta.ca).

Digital Object Identifier 00.0000/LAWP.0000.0000000

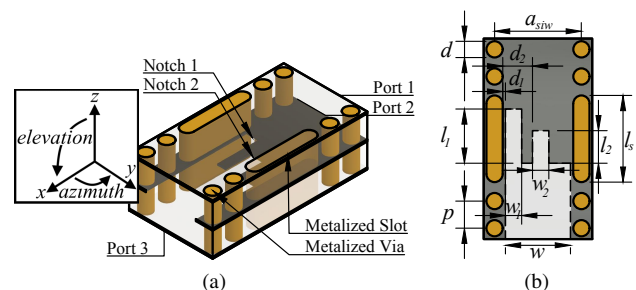


Fig. 1. Structure of the notched-septum SIW polarizer. (a) Isometric view. (b) Top view.

TABLE I
PARAMETERS OF THE NOTCHED-SEPTUM SIW POLARIZER

Parameter Value (mm)	d_1	l_1	w_1	d_2	l_2	w_2
Parameter Value (mm)	0.18	1.45	0.15	2.03	1.32	0.30
Parameter Value (mm)	a_{siw}	p	d	w	l_s	
	4.50	1.20	1.00	3.43	3.35	

In this letter, an SIW notched-septum polarizer is presented, with a focus on minimizing size and improving tolerance to manufacturing variations. While the SIW notched-septum polarizer will provide a narrower AR bandwidth compared to other septum polarizers, it will be sufficient for anticipated 5G bands while being compact (much smaller than λ_o) and easy to integrate with other parts, making it a candidate for use in SIW CP endfire antennas in 5G handheld devices (demonstrated through its implementation in a 4-elements array antenna).

II. DESIGN PROCESS

The proposed polarizer is shown in Fig. 1 and associated dimensions are listed in Table I. It is a 3-port device with two ports (P1 and P2) capable of propagating only TE_{10} modes, and the third port (P3) capable of propagating TE_{10} and TE_{01} modes (and thus able to transmit/receive circularly polarized, CP, fields). This is demonstrated by the propagation constant of the various modes at the three ports in Fig. 2(a), with Fig. 2(b) illustrating the E-field orientation of the main modes considered. The theoretical maximum band of operation is from 22 GHz to 30 GHz, with the lower band edge being dictated by the cutoff frequency of the intended modes, and the upper band edge being limited by the cutoff frequency of the TE_{11} and TM_{11} modes. The polarizer is implemented as two substrate-integrated waveguides (SIWs), with thicknesses of 1.8 mm each, stacked on top of each other with a shared broad

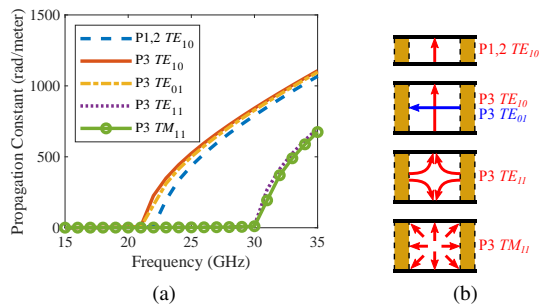


Fig. 2. Modes in the three ports of the polarizer. (a) Propagation constant. (b) Field configuration.

wall. The dielectric is Rogers RO4350B ($\epsilon_r = 3.66$ and $\tan \delta = 0.0037$) given its compatibility with PCB manufacturing processes. The use of the dielectric also plays a role in the reduction of size (compared to an air-filled waveguide). The shared wall between the two SIWs ends abruptly. Two notches are cut into them. Metalized vias along the SIWs act as the walls to the waveguides. Specifically, around where the notches are, the metalized vias are replaced with metalized slots to limit the effects of non-ideal metal walls on the polarization process, to ensure better polarization purity. Furthermore, the design of the notches takes into account the limitations of PCB manufacturing and ensures tolerance to any variations. The septum length is dictated by the longest notch and is thus only $\lambda_o/7$ long. To achieve CP at P3, we require both TE_{10} and TE_{01} modes with identical amplitudes, and in-quadrature. Any quadrature phase deviation and amplitude error would result in decreased CP purity as quantified in [11]

$$AR = \sqrt{A_e^2 + 0.0225\phi_e^2} \quad [\text{dB}] \quad (1)$$

where A_e is the amplitude difference between the modes in P3 and ϕ_e is the deviation from quadrature phase of the two modes in P3, both defined as

$$A_e = A_1 - A_2 \quad [\text{dB}] \quad (2)$$

$$\phi_e = 90 - |\phi_1 - \phi_2| \quad [\text{deg}] \quad (3)$$

where subscripts 1 and 2 are for the TE_{10} and TE_{01} modes of P3, respectively.

To analyze a polarizer with a narrow single notch (which can only support E_y fields), we will examine scattered fields resulting from theoretical excitation of TE_{10} and TE_{01} modes at P3, individually (as in [12]). First, we consider the excitation of TE_{10} at P3. The fields will propagate through, unaffected by the septum and couple equally to TE_{10} modes at P1 and P2. Next, TE_{01} fields at P3 cannot propagate into the rectangular SIWs, and can only either couple to the notch or be reflected. Reflected fields determine impedance matching. Fields coupled to the notch result in scattered fields on either sides of the septum (analogous to a slot antenna). Given the symmetry of the structure (with respect to the notch), resultant E_z fields in both rectangular SIWs point in opposite directions. The resultant fields are thus TE_{10} modes at P1 and P2 (but with 180° phase difference between them). Furthermore, compared to the resultant fields from just a TE_{10} excitation

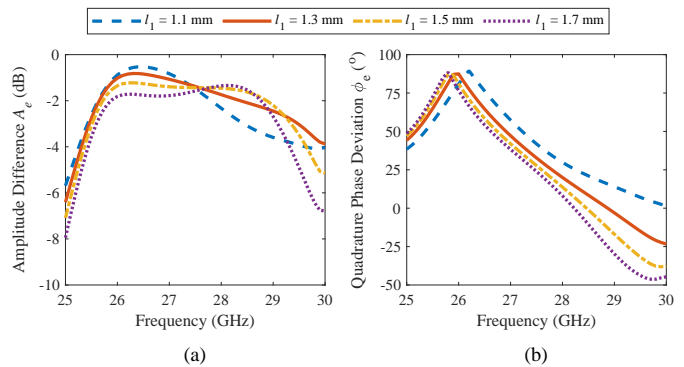


Fig. 3. Simulated parametric sweep of notch 1 length l_1 . (a) Amplitude error A_e . (b) Quadrature phase deviation ϕ_e .

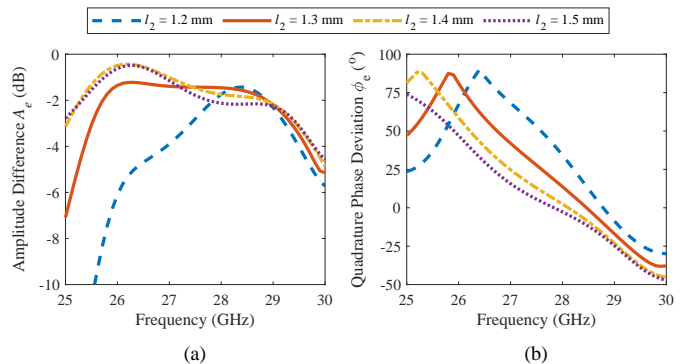


Fig. 4. Simulated parametric sweep of notch 2 length l_2 . (a) Amplitude error A_e . (b) Quadrature phase deviation ϕ_e .

at P3, these resultant fields demonstrate a phase shift resulting from the scattering mechanism of the notch.

The analysis results will apply (in reverse) when considering excitation of TE_{10} fields at P1 and/or P2 given that the structure is passive and bidirectional. Therefore, exciting P1 and P2 equally (in amplitude and phase) will result in a purely TE_{10} mode at P3, whereas, exciting fields with 180° offsets at P1 and P2 will result in a purely TE_{01} mode at P3. Exciting only P1/P2 is a superposition of the two excitation cases previously mentioned. The resultant fields at P3 will thus be a combination of TE_{10} and TE_{01} modes with a phase offset and amplitude difference between them dictated by the notch. Despite having three design variables (length, width and position) and three metrics to design for (impedance matching, amplitude difference and phase offset), the requirement of a narrow notch limits our degree of freedom to less than the three required by the metrics. In order to better meet those requirements, we introduce a second notch. Besides the non-ideality due to coupling between the two notches, the second notch's operation should follow that of the single notch described above, with added flexibility.

It is more efficient to optimize the design (with initial parameters) than to solve for scattered fields. To avoid running optimizations for six variables, the lengths of both notches were set, with $l_1 = 1.45$ mm ($\lambda_o/7$) and $l_2 = 1.32$ mm. Given that the notches can only support E_y fields, their lengths can be set such that quadrature phase can be achieved. This is

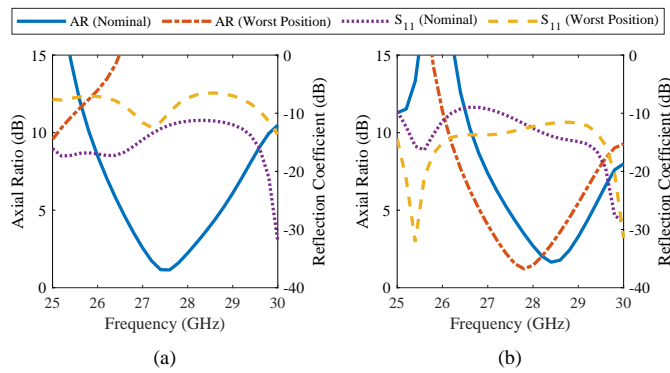


Fig. 5. Simulated AR and S_{11} of the initial notched-septum polarizer ($l_1 = 1.45$ mm, $l_2 = 1.32$ mm, $w_1 = 0.15$ mm) with and without worst-case metalized slots' size & position. (a) $w_2 = 0.35$ mm, $d_1 = 0.05$ mm, and $d_2 = 1.81$ mm. (b) $w_2 = 0.30$ mm, $d_1 = 0.18$ mm, and $d_2 = 2.03$ mm.

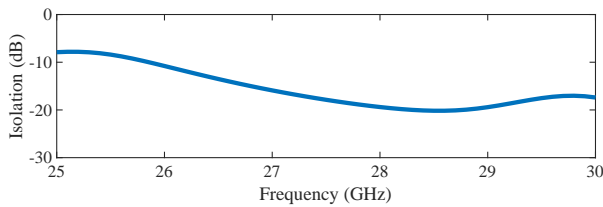


Fig. 6. Simulated isolation between P1 and P2 of the polarizer.

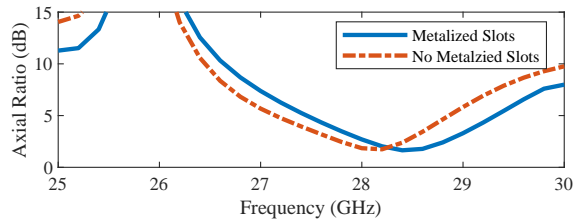


Fig. 7. Simulated AR of the notched-septum polarizer with and without metalized slots in the vicinity of the notches.

demonstrated in the l_1 and l_2 parametric sweeps in Fig. 3 and Fig. 4 (respectively), whereby greater notch lengths result in greater E_y phase. Notch lengths also affect amplitudes, thus requiring optimization with the other variables. An optimal AR bandwidth (BW), centered at 28 GHz, is achieved for an initial set of parameters as shown in Fig. 5(a). However, given typical manufacturing tolerances, there is the possibility that the metalized slot would go through the first notch. Furthermore, annular rings are required around vias and slots. Thus the notches are further optimized within those restrictions, at the expense of a shift in center frequency as shown in Fig. 5(b). In the same figure, the polarizer is shown to be resilient to variations in the slots' position, displaying only a frequency shift. Finally, as shown in Fig. 6, 20 dB isolation is observed between P1 and P2 within the band of operation.

One design feature is the use of metalized slots in the vicinity of the polarizer rather than vias to ensure a flatter amplitude error between P3's two modes. This is demonstrated in Fig. 7 where a wider AR BW is achieved.

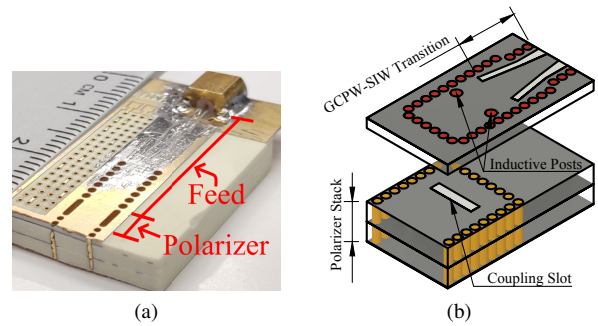


Fig. 8. (a) Photograph of half of the back-to-back polarizer. (b) Feed design.

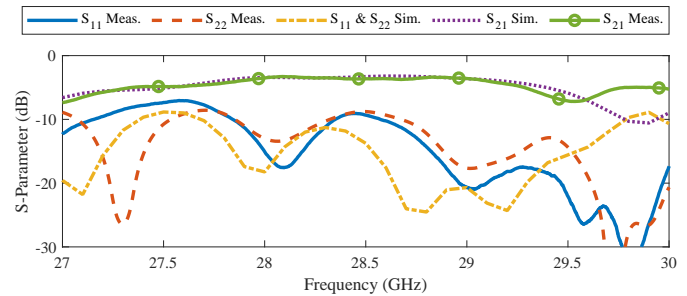


Fig. 9. Measured and simulated reflection and transmission coefficients of the back-to-back polarizer.

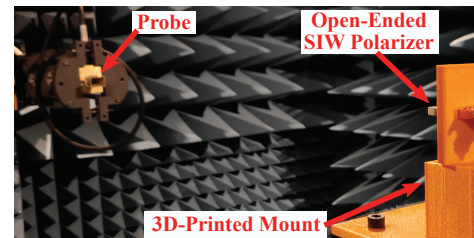


Fig. 10. Anechoic chamber setup to measure AR of the polarizer.

III. MEASUREMENT

A back-to-back implementation of the polarizer is manufactured as shown in Fig. 8(a). The top ports of each polarizer are coupled through slots to SIWs on a 0.5 mm layer above as shown. The SIWs then transition to grounded coplanar waveguides for soldering of SMP connectors as shown in Fig. 8(b). The simulated and measured S-parameters of the polarizer are shown in Fig. 9, where ports 1 and 2 are at the SMP connectors. The simulated and measured single polarizer transmission coefficients are both seen to be approximately -1.6 dB, with part of the loss being attributed to the additional structures added to facilitate testing. While a simulated impedance matching BW of 7.1% at 28.6 GHz is achieved, the measured matching BW is 7.9% at 29 GHz, with a peak to -9 dB at 28.5 GHz. The shift in frequency is attributed to fabrication and ϵ_r error, and imperfect connector soldering.

The polarizer AR is measured in an NSI-MI anechoic chamber as shown in Fig. 10, with the polarizer radiating with an open-ended SIW. The rectangular measuring probe is operated in horizontal and vertical orientations to measure the far-field boresight gain and phase of the orthogonal fields.

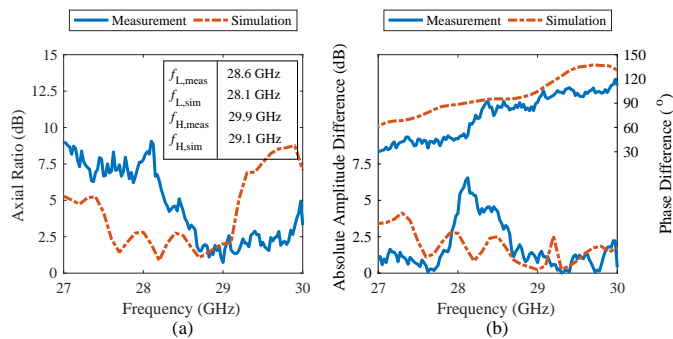


Fig. 11. Polarizer results. (a) Measured and simulated AR. (b) Measured and simulated amplitude and phase differences.

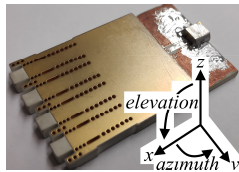


Fig. 12. Photograph of the 4-element array (a use case of the polarizer).

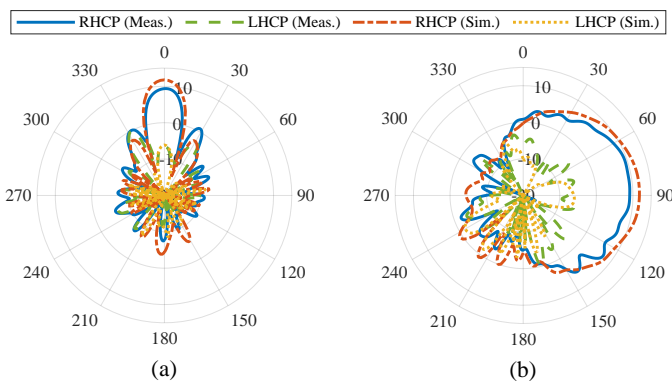


Fig. 13. Far-field simulated and measured RHCP and LHCP radiation patterns of the 4-element array with polarizer at center frequency. (a) Azimuth plane. (b) Elevation plane.

The simulation and measurement far-field ARs are shown in Fig. 11(a). The simulated AR is demonstrated to be ≤ 3 dB from 28 GHz to 29.1 GHz, whereas it is observed to be ≤ 3 dB from 28.6 GHz to 29.9 GHz in measurement. While the BW size is identical, a frequency shift of 2.5% is observed. This is identical to the shift observed in impedance matching BW. Beyond the reasoning provided earlier, there is also a tight alignment tolerance of the antennas in the measurement setup. The frequency shift can be addressed in future designs by taking it into consideration. Measured and simulated differences in amplitude and phase (between the two linear components) are shown in Fig. 11(b). The shift in AR BW can be attributed to a shift in both amplitude and phase differences. It is also observed that, within the measured AR BW, the phase difference is within $\pm 15^\circ$ of 90° , while the absolute amplitude difference is at worse 3 dB (at 28.6 GHz). The AR BW is thus dictated by amplitude difference at the lower frequency end, whereas it is dictated by a combination of both phase and amplitude differences at the higher frequency.

TABLE II
COMPARISONS OF DIFFERENT POLARIZERS

Ref.	f_c (GHz)	Size $L \times W \times H$ (λ_0^3)	IM [†] BW (%)	AR BW (%)	FOM* ($\frac{\%}{\lambda_0^3}$)
[6]	5.8	$1.47 \times 0.79 \times 0.79$ $1.53 \times 0.79 \times 0.79$	>29 >22	>25 >15	>27.3 >15.7
[7]	60.2	$0.71 \times 0.58 \times 0.72$	7.8	0.3	1.0
[8]	21	$1.19 \times 1.85 \times 0.22$	40.5	>42.9	83.6
[12]	15.2	$0.37 \times 0.80 \times 0.80$	6.4	3.7	15.6
[14]	18.7	$1.60 \times 0.66 \times 0.27$	>26.7	1.8	6.31
[15]	94.1	$1.76 \times 1.49 \times 0.25$	31.5	34.7	48.0
[16]	37.5	$0.66 \times 0.69 \times 0.38$	29.3	22.5	130.0
[17]	28	$2.26 \times 0.28 \times 0.56$	42.9	27.9	78.7
This Work	29	$0.14 \times 0.53 \times 0.35$	7.9	4.5	173.2

[†] Impedance Matching * Figure of Merit: $\frac{\min(BW)}{L \times W \times H}$

In order to illustrate the effectiveness of the polarizer for CP endfire radiation, it is incorporated within an array of four elements as shown in Fig. 12. The array consists of a splitter, polarizers and dielectric lenses, all in SIW technology [13]. The array is measured in the NSI-MI anechoic chamber. The simulated and measured right-hand and left-hand CP (RHCP and LHCP) radiation patterns (in azimuth and elevation) are shown in Fig. 13. Besides the difference in gain, simulated and measured results are in close agreement. The array demonstrates pure RHCP within the azimuth and elevation half-power beamwidths, thus confirming the functionality of the proposed polarizer as a part of an entire 5G system.

The polarizer is compared to other compact polarizers, in Table II, to examine its merits. For works that present polarizers within a system, only the polarizer is considered for size. Given the compromise between size and performance, a figure of merit (FOM), which considers the size and minimum BW of the polarizer, is included. While the operable BW of the proposed polarizer is among the smallest, its minimal footprint results in the best FOM. Furthermore, the achieved AR BW of 4.5% is wider than proposed BW sizes (of $\leq 3\%$) for 5G communications, thus there is no lost functionality. Finally, in comparison to the waveguide notched-septum polarizer [12], our polarizer demonstrates a 9.1x improvement in size, with 7x being due to the use of the dielectric and 1.3x due to the notches and metalized slots (both of which also improve AR BW by 1.2x).

IV. CONCLUSION

In this letter, an SIW notched-septum polarizer is presented. Two notches are employed for the generation of CP when either of the two input rectangular SIWs are excited. The notches are designed such that the polarizer is tolerant to typical PCB manufacturing variations. Metalized vias along the notches are replaced with metalized slots for a wider AR BW. A back-to-back polarizer demonstrates an impedance matching BW of 7.9% at 29 GHz, with a single polarizer transmission coefficient of -1.6 dB. The polarizer achieves a 3 dB AR BW of 4.5% at 29 GHz. Given its performance and size, the polarizer is a candidate for SIW CP endfire antennas in 5G mobile devices.

REFERENCES

- [1] Y. Cao, Y. Cai, L. Wang, Z. Qian, and L. Zhu, "A review of substrate integrated waveguide end-fire antennas," *IEEE Access*, vol. 6, pp. 66 243–66 253, 2018.
- [2] W. Hong, S.-T. Ko, Y. Lee, and K. H. Baek, "Compact 28 GHz antenna array with full polarization flexibility under yaw, pitch, roll motions," in *2015 9th European Conference on Antennas and Propagation (EuCAP)*, Lisbon, Portugal, May 2015, pp. 1–3.
- [3] A. Li, K. Luk, and Y. Li, "A dual linearly polarized end-fire antenna array for the 5G applications," *IEEE Access*, vol. 6, pp. 78 276–78 285, 2018.
- [4] A. J. Simmons, "Phase shift by periodic loading of waveguide and its application to broad-band circular polarization," *IRE Transactions on Microwave Theory and Techniques*, vol. 3, no. 6, pp. 18–21, December 1955.
- [5] M. Chen and G. Tsandoulas, "A wide-band square-waveguide array polarizer," *IEEE Transactions on Antennas and Propagation*, vol. 21, no. 3, pp. 389–391, May 1973.
- [6] I. Kim, J. M. Kovitz, and Y. Rahmat-Samii, "Enhancing the power capabilities of the stepped septum using an optimized smooth sigmoid profile," *IEEE Antennas and Propagation Magazine*, vol. 56, no. 5, pp. 16–42, Oct 2014.
- [7] X. Cheng, Y. Yao, T. Tomura, J. Hirokawa, T. Yu, J. Yu, and X. Chen, "A compact multi-beam end-fire circularly polarized septum antenna array for millimeter-wave applications," *IEEE Access*, vol. 6, pp. 62 784–62 792, 2018.
- [8] M. Farshahi, E. Zareian-Jahromi, and R. Basiri, "A compact wideband circularly polarized SIW horn antenna for K band applications," *AEU - International Journal of Electronics and Communications*, vol. 99, pp. 376 – 383, 2019. [Online]. Available: <http://www.sciencedirect.com/science/article/pii/S1434841118319836>
- [9] F. M. Monavar, S. Shamsinejad, R. Mirzavand, J. Melzer, and P. Mousavi, "Beam-steering SIW leaky-wave subarray with flat-topped footprint for 5G applications," *IEEE Transactions on Antennas and Propagation*, vol. 65, no. 3, pp. 1108–1120, March 2017.
- [10] W. El-Halwagy, R. Mirzavand, J. Melzer, M. Hossain, and P. Mousavi, "A substrate-integrated fan-beam dipole antenna with varied fence shape for mm-wave 5G wireless," in *2018 IEEE International Symposium on Antennas and Propagation USNC/URSI National Radio Science Meeting*, July 2018, pp. 251–252.
- [11] S. V. Parekh, "Simple formulae for circular-polarization axial-ratio calculations," *IEEE Antennas and Propagation Magazine*, vol. 33, no. 1, pp. 30–32, Feb 1991.
- [12] N. C. Albertsen and P. Skov-Madsen, "A compact septum polarizer," *IEEE Transactions on Microwave Theory and Techniques*, vol. 31, no. 8, pp. 654–660, Aug 1983.
- [13] K. Al-Amoodi, M. M. Honari, R. Mirzavand, J. Melzer, D. G. Elliott, and P. Mousavi, "Circularly-polarised end-fire antenna and arrays for 5G millimetre-wave beam-steering systems," *IET Microwaves, Antennas and Propagation*, April 2020. [Online]. Available: <https://digital-library.theiet.org/content/journals/10.1049/iet-map.2019.1119>
- [14] Y. Cai, Y. Zhang, Z. Qian, W. Cao, and S. Shi, "Compact wideband dual circularly polarized substrate integrated waveguide horn antenna," *IEEE Transactions on Antennas and Propagation*, vol. 64, no. 7, pp. 3184–3189, July 2016.
- [15] X. Cheng, Y. Yao, J. Yu, and X. Chen, "Circularly polarized substrate-integrated waveguide tapered slot antenna for millimeter-wave applications," *IEEE Antennas and Wireless Propagation Letters*, vol. 16, pp. 2358–2361, 2017.
- [16] Q. Wu, J. Hirokawa, J. Yin, C. Yu, H. Wang, and W. Hong, "Millimeter-wave multibeam endfire dual-circularly polarized antenna array for 5G wireless applications," *IEEE Transactions on Antennas and Propagation*, vol. 66, no. 9, pp. 4930–4935, Sep. 2018.
- [17] Y. Zhang, Y. Jiao, and L. Zhang, "Wideband inhomogeneous-polarizer loaded circularly polarized SIW horn antenna for broadband millimeter-wave applications," *IEEE Antennas and Wireless Propagation Letters*, vol. 18, no. 7, pp. 1448–1452, July 2019.